

Origin of magnetic moments in defective TiO₂ single crystals

Shengqiang Zhou,^{1,*} E. Čížmár,² K. Potzger,¹ M. Krause,¹ G. Talut,¹
M. Helm,¹ J. Fassbender,¹ S. A. Zvyagin,² J. Wosnitza,² and H. Schmidt¹

¹*Institute of Ion Beam Physics and Materials Research, Forschungszentrum Dresden-Rossendorf, 01314 Dresden, Germany*

²*Dresden High Magnetic Field Laboratory (HLD), Forschungszentrum Dresden-Rossendorf, 01314 Dresden, Germany*

(Dated: November 15, 2018)

In this paper we show that ferromagnetism can be induced in pure TiO₂ single crystals by oxygen ion irradiation. By combining x-ray diffraction, Raman-scattering, and electron spin resonance spectroscopy, a defect complex, *i.e.* Ti³⁺ ions on the substitutional sites accompanied by oxygen vacancies, has been identified in irradiated TiO₂. This kind of defect complex results in a local (TiO_{6-x}) stretching Raman mode. We elucidate that Ti³⁺ ions with one unpaired 3d electron provide the local magnetic moments.

Recently, ferromagnetism has been observed in non-magnetically doped, but defective oxides, including TiO₂^{1,2,3,4}. This kind of observation challenges the conventional understanding of ferromagnetism, which is rather due to spin-split states or bands. Thus, one fundamental question must be answered: where are the moments located? Intensive theoretical work has been performed to understand the ferromagnetism in defective oxides^{5,6,7}. In these papers, the triplet states of p-like electrons, located at cation or oxygen vacancies, yield the local moments, leading to a kind of ferromagnetism without the involvement of 3d electrons. Experimentally the ferromagnetism in undoped TiO₂ has been found to relate with oxygen vacancies (O_V)^{2,3}, however, its mechanism remains unclear. It is worth to note that Ti³⁺ ions with one 3d electron are usually generated in slightly reduced TiO₂. When O is removed, the excess electrons are unpaired⁸. They can occupy the nearby localized Ti 3d orbit and therefore convert Ti⁴⁺ ions to Ti³⁺ ions. In a reduced rutile TiO₂(110) surface, such a defect complex, Ti³⁺-O_V, has been well studied by first-principles calculations^{9,10} and experimentally by resonant photoelectron diffraction¹¹. Therefore, experimental work is needed to clarify whether the magnetic moments in defective TiO₂ is due to unpaired 3d electrons localized on Ti³⁺ ions.

Ion irradiation is a non-equilibrium and reproducible method of inducing defects. Energetic ions displace atoms from their equilibrium lattice sites, thus creating mainly vacancies and interstitials. The amount of defects can be controlled by the ion fluence and energy. In this paper, we irradiated rutile TiO₂ single crystals with 2-MeV O ions, resulting in a projected range of 1.52 μm and a longitudinal straggling of 0.16 μm as calculated by SRIM code (The Stopping and Range of Ions in Matter)¹². As a result of this irradiation, the formation of Ti/O vacancies/interstitials is expected¹². We selected high-energy oxygen ions as projectiles to avoid the introduction of foreign elements. Moreover, from a ballistic point of view, the creation of oxygen vacancies is more efficient, *e.g.*, by a factor of 1.5 larger than the Ti-vacancy creation. From SRIM calculations it is also evident that, at the given energy, the maximum atomic

concentration of the implanted oxygen ions is by a factor of 500 smaller than the concentration of oxygen recoils. For the region of maximum defect creation, *i.e.*, at the end of the ion range, those projectiles play no chemical role. Thus, the desired local oxygen deficiency can be obtained by the proposed experimental procedure. The selection of TiO₂ single crystals instead of thin films is expected to exclude any effect of possible magnetic impurities in the underlying substrates¹³, and of the interfaces between films and substrates¹⁴.

Commercial rutile TiO₂ single crystals were irradiated with 2 MeV O ions at room temperature with fluences from 1×10^{15} to $5 \times 10^{16} \text{ cm}^{-2}$. All samples are from the same purchase charge with an equal size of $5 \times 5 \times 0.5 \text{ mm}^3$, corresponding to a mass of 53 mg. The samples thereafter were named as 1E15, ..., 5E16. All samples were investigated using SQUID magnetometry (Quantum design MPMS-7XL), X-ray diffraction (XRD, Siemens D5005), Raman spectroscopy (LabramHR, Jobin-Yvon-Horiba) and electron spin resonance (ESR, Bruker ELEXSYS E500 at 9.4 GHz). SQUID measurements indicate that the virgin TiO₂ single crystals are weak paramagnets with a susceptibility of $7.7 \times 10^{-6} \text{ emu/T}\cdot\text{g}$.

Fig. 1(a) shows the measured magnetic moment of TiO₂ at 300 K before and after irradiation with a fluence of $5 \times 10^{15} \text{ cm}^{-2}$. After irradiation the sample shows a ferromagnetic hysteresis added to the linear paramagnetic background. The saturation magnetic moment is in the order of 10^{-5} emu , well above the sensitivity limit of SQUID magnetometry. The inset shows the low-field part in an enlarged scale. The coercive field of around 10 mT can be clearly resolved. Fig. 1(b) shows the irradiation-fluence dependent magnetic moment of TiO₂ single crystals after subtracting the linear paramagnetic background. The magnetic moment first increases drastically with increasing fluence, but for the fluences above $5 \times 10^{15} \text{ cm}^{-2}$ it decreases significantly again. For the 5E15 sample, with the largest magnetic moment, we also measured the hysteresis loops at different temperatures (not shown). The loops are weakly temperature dependent. This is also a feature of the reported defect-induced ferromagnetism¹⁵.

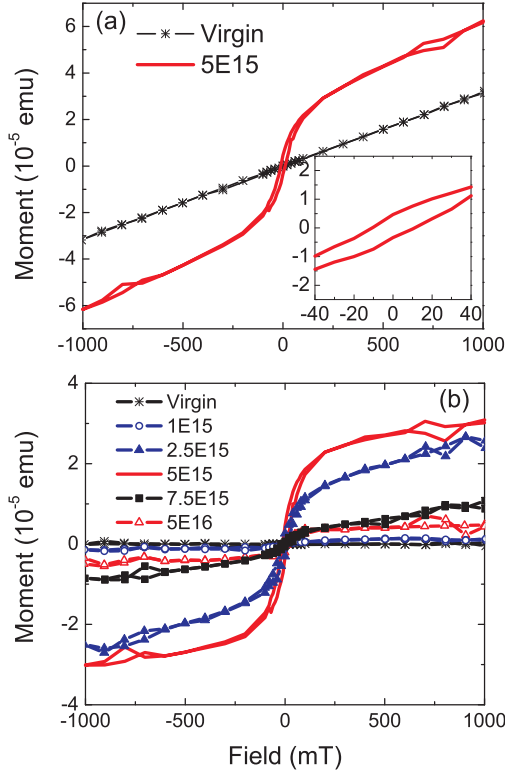


FIG. 1: (Color online) (a) Magnetic moments measured at 300 K as a function of magnetic field before and after irradiation. Inset: the low-field part of the loop for sample 5E15. (b) Magnetic moments at 300 K for samples with an equal sample-size and different ion fluences. The linear paramagnetic background has been subtracted.

The structural evolution upon ion irradiation was assessed by X-ray diffraction (XRD) and Raman-scattering measurements. Fig. 2(a) shows the XRD patterns close to the $\text{TiO}_2(330)$ peak before and after irradiation at different fluences. One remarkable characteristic is that a new peak appears at the left side of the (330) peak after irradiation. This new peak is induced by a strained TiO_2 layer with a larger lattice spacing compared to that of the virgin TiO_2 . With increasing fluence, this peak shifts towards smaller 2θ angles and arrives at a minimum at a fluence of $7.5 \times 10^{15} \text{ cm}^{-2}$. The largest strain is around 0.50%, however the peak becomes weaker. With further increasing fluence, the peak finally disappears and develops into a gradual shoulder, which means the loss of crystalline long-range ordering of the irradiated layer. This phenomenon is usually due to the fact that with increasing density point defects accumulate and develop into extended defects, e.g., dislocations. The lattice expansion upon ion irradiation is a common feature in semiconductors, e.g., in GaN¹⁶.

The effect of oxygen implantation on the structural properties of TiO_2 was further studied by Raman spectroscopy. The experiments were carried out in a micro Raman 180° backscattering geometry. The scattering in-

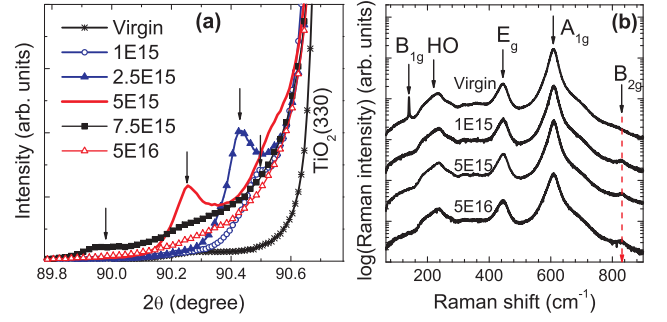


FIG. 2: (Color online) (a) XRD pattern for O-irradiated TiO_2 . The peaks (marked by arrows) in the left side of the $\text{TiO}_2(330)$ peak evidence the irradiation-generated strain in TiO_2 . (b) Raman spectra of TiO_2 single crystals after oxygen ion irradiation with different fluences. The spectra are shifted vertically for better visualization. A clear mode at the range of B_{2g} (as indicated by the dashed arrow) has been observed after irradiation.

tensities were measured using vertical orientation of the crystal $[110]$ -axis relative to the electric field vector of the incoming laser. The spectrum of the virgin sample [Fig. 2(b)] shows four distinct lines which are assigned to the B_{1g} (143 cm^{-1}), E_g (447 cm^{-1}), and A_{1g} (612 cm^{-1}) fundamental modes and to a higher order (HO) band around 234 cm^{-1} of rutile TiO_2 ¹⁷. The fourth Raman-active fundamental mode with B_{2g} symmetry appears as a weak shoulder at 820 cm^{-1} . Neither the fingerprint lines from the anatase TiO_2 at 144 cm^{-1} nor those of Ti_2O_3 at 269 cm^{-1} and at 347 cm^{-1} have been observed in the irradiated samples^{18,19,20}. Already at the smallest fluence, the irradiation induces i) the complete disappearance of B_{1g} and ii) significant changes in the range of the B_{2g} mode, where instead of the shoulder at 820 cm^{-1} a clearly resolved line appears at 834 cm^{-1} [indicated by the dashed arrows in Fig. 2(b)]. The B_{1g} mode is very sensitive to the long-range order of TiO_2 crystals. It softens when applying high pressure and loses intensity much faster than the other fundamental modes²⁰. Raman spectra of micro- and nanocrystalline TiO_2 of 5 nm to $2 \mu\text{m}$ average crystallite size did not show the B_{1g} mode as reported recently²¹. An important conclusion of the complete absence of B_{1g} is that the information depth of the Raman spectra is limited to the irradiated part of the sample. The integrated intensity of the line at 834 cm^{-1} is ~ 5.5 times larger than that of the corresponding shoulder for a virgin TiO_2 . In virgin TiO_2 the B_{2g} mode represents an asymmetric (Ti-O) stretching vibration of the (TiO_6) -octahedra (Ti ions are surrounded by six O ions)²¹. It is therefore sensitive to the short-range order and the bond strength in the crystal, i.e., the local environment of the Ti ions. Since a reduction of the crystallite size usually causes red-shifts of vibrational modes, the observed blue-shift by 14 cm^{-1} of the B_{2g} mode cannot be explained by phonon confinement. Furthermore, the line can be neither assigned to an IR-active nor to a silent mode of rutile TiO_2 possibly activated due to a crystal-symmetry

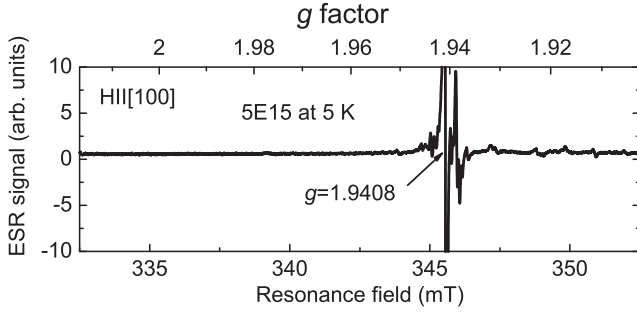


FIG. 3: ESR signals observed in sample 5E15 at 5 K. The applied field is along the [100] axis. The main ESR peak accompanied by a hyperfine interaction pattern has a g -factor of 1.9408.

reduction²². The line at 834 cm^{-1} indicates a stronger bond between the Ti and the O atoms than in the virgin rutile. One possible reason is the reduced coordination number of Ti ions resulting in TiO_{6-x} instead of TiO_6 , since a lower coordination number leads to bond contraction and higher vibrational frequencies. This mechanism should in principle also affect the other Raman lines, particularly the A_{1g} mode. However, a possible high-energy shoulder would be easily hidden under the large scattering intensity of the main components. The localized origin of the mode at 834 cm^{-1} is also supported by the dependence of the Raman line parameters on implantation fluences. While the A_{1g} and E_g lines are broadened with increasing oxygen fluence due to irradiation-induced defects, the local (TiO_{6-x}) stretching mode shows a slight line narrowing. Therefore, we conclude that oxygen irradiation results in the local distortion of the overall TiO_6 coordination, which gives rise to a local TiO_{6-x} stretching mode in the range of the B_{2g} mode. Such a distorted TiO_{6-x} octahedral has also been considered in a recent experimental and molecular dynamics simulation study of ion irradiation damage in TiO_2 ²³.

In order to understand the origin of the local moments, ESR measurements were performed on the virgin and two selected irradiated samples: 5E15 (with the largest magnetic moment), and 5E16 (with the largest irradiation fluence). ESR directly probes the interaction between unpaired electrons and the magnetic field. In a broad applied field range from 50 mT to 550 mT along the $\text{TiO}_2[100]$ axis and with temperatures down to 5 K, we only detected one ESR peak at a g -factor of 1.9408 accompanied by a complicated hyperfine interaction pattern for the two irradiated samples. Fig. 3 shows the featured field-range of the measured ESR spectrum at 5 K for sample 5E15. Note that electrons trapped by vacancies have a g -factor slightly larger than 2 and exhibit no hyperfine features^{24,25}. The lineshape (see Fig. 4 for details) and the g -factor are typical features in the so-called A spectrum due to Ti^{3+} ions^{26,27}. Now we come to the question: how the Ti^{3+} ions are generated after irradiation? Among the defects created by irradiation, only O vacancies and Ti interstitials can contribute ex-

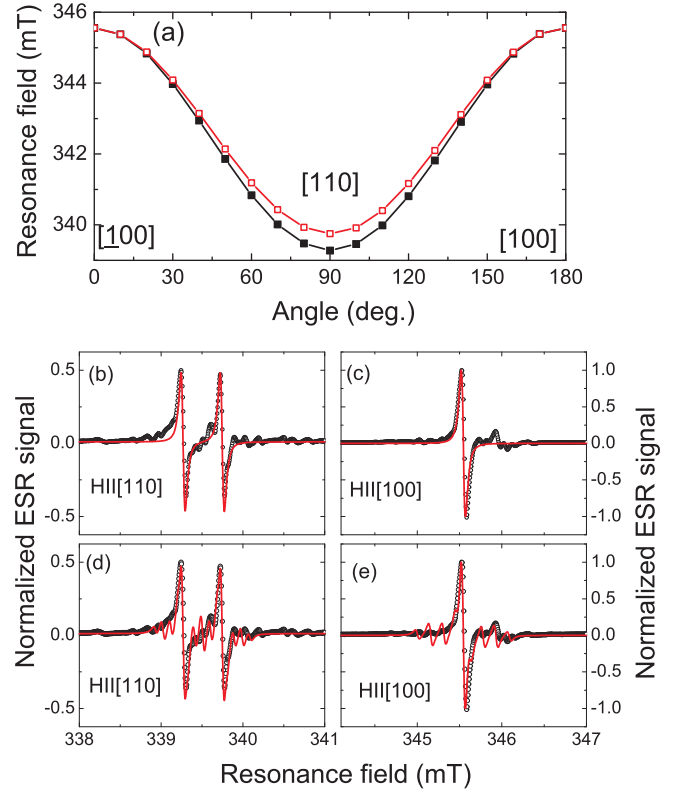


FIG. 4: (Color online) (a) Angular-dependent resonance field of the ESR spectrum: it is split into two lines upon field orientation changing from the [100] to the [110] axis. (b)-(e) Comparison between simulated (solid lines) and measured (open circles) ESR data. (b) and (d): With field along the [110] direction without (b) and with (d) considering hyperfine interaction. (c) and (e): With field along the [100] direction without (c) and with (e) considering hyperfine interaction.

cess electrons^{8,28}. There are three factors favoring the formation of $\text{Ti}^{3+}\text{-O}_V$ defect complexes: (1) As the nearest neighbors O vacancies are more close to substitutional Ti ions, (2) the number of O vacancies is 1.5 times larger than that of Ti interstitials¹² and (3) energetically the formation of O vacancies is slightly favored over the formation of Ti interstitials⁸. Therefore we can conclude that each of irradiation-induced oxygen vacancies leaves two electrons and converts the neighboring Ti^{4+} to Ti^{3+} ions, resulting in $\text{Ti}^{3+}\text{-O}_V$ defect complexes. Such a converting in the reduced $\text{TiO}_2(110)$ surface has been confirmed recently by both theoretical and experimental works^{10,11}. It is important to note that the virgin sample shows no detectable ESR line down to 5 K (not shown) since the virgin TiO_2 contains no unpaired electrons.

The site occupation of the Ti^{3+} ions, namely substitutional or interstitial, is determined by the angular dependence of the A spectrum. The crystalline symmetry results in a two-fold splitting of the Ti^{3+} ESR lines at substitutional sites, and a four-fold splitting at interstitial sites, when the field orientation is changed from the [100] to the [110] axis²⁷. As shown in Fig. 4(a), we can

conclude that the Ti^{3+} ions in our samples occupy substitutional sites. We performed a simulation of the ESR spectra with this assumption as shown in Fig. 4(b)-(e). For fields along [110] and [100] and with the anisotropic g -factors $[g_x, g_y, g_z] = [1.9408, 1.9738, 1.9766]$, we obtained the spectra as shown in Fig. 4(b)-(d). Without considering the hyperfine interaction, the simulated spectra agree reasonably well with the experimental data in g -factor, lineshape, and splitting with field rotation. When taking the hyperfine interaction into account, namely the nuclear spin of ^{47}Ti ($I = 5/2$) and ^{49}Ti ($I = 7/2$), the simulations reproduce the experimental results even much better.

The presence of Ti^{3+} at substitutional sites also explains the XRD results considering the fact that substitutional Ti^{3+} ions are larger than Ti^{4+} ions resulting in the observed lattice expansion. However, the other point defects, i.e. Ti/O interstitials can also result in the lattice expansion. Combining the findings of Raman and ESR measurements, we conclude the following. Among the various defects created by oxygen ion irradiation, Ti^{3+} ions on substitutional sites are accompanied by oxygen vacancies (O_V) forming defect complexes, which result

in a local (TiO_{6-x}) stretching Raman mode. When the ion fluence is very large, the irradiated layer loses its long-range crystalline ordering, such that the fundamental mode of TiO_2 is broadened.

Summarizing our results, we conclude that (1) a Ti^{3+} - O_V defect complex is generated due to ion irradiation. The Ti^{3+} ions provide local $3d$ moments which are decisively related with the observed ferromagnetism; (2) There is an optimum fluence to produce enough Ti^{3+} ions while keeping the crystalline ordering. Since ESR is not capable to determine the concentration of Ti^{3+} ions, it is difficult to get a quantitative insight of the magnetic coupling mechanism. Despite such an unfolded question, our research suggests that the combination of ion irradiation and ESR techniques can be a general approach to verify the predicted defect-induced ferromagnetism in oxides^{6,29}. The simultaneous observation of ferromagnetism and ESR signal with a g -factor slightly above 2 would be the criterion.

The authors (S.Z. and H.S.) acknowledge financial funding from the Bundesministerium für Bildung und Forschung (FKZ03N8708).

-
- * Electronic address: S.Zhou@fzd.de
- ¹ J. M. D. Coey, M. Venkatesan, P. Stamenov, C. B. Fitzgerald, and L. S. Dorneles, *Phys. Rev. B* **72**, 024450 (2005).
 - ² S. D. Yoon, Y. Chen, A. Yang, T. L. Goodrich, X. Zuo, D. A. Arena, K. Ziemer, C. Vittoria, and V. G. Harris, *J. Phys.: Condens. Matter* **18**, L355 (2006).
 - ³ N. H. Hong, J. Sakai, N. Poirot, and V. Brizé, *Phys. Rev. B* **73**, 132404 (2006).
 - ⁴ S. Zhou, K. Potzger, G. Talut, H. Reuther, K. Kuepper, J. Grenzer, Q. Xu, A. Mücklich, M. Helm, J. Fassbender, E. Arenholz, *J. Phys. D: Appl. Phys.* **41**, 105011 (2008).
 - ⁵ I. S. Elfimov, S. Yunoki, and G. A. Sawatzky, *Phys. Rev. Lett.* **89**, 216403 (2002).
 - ⁶ J. Osorio-Guillén, S. Lany, S. V. Barabash, and A. Zunger, *Phys. Rev. Lett.* **96**, 107203 (2006).
 - ⁷ T. Chanier, I. Opahle, M. Sargolzaei, R. Hayn, and M. Lannoo, *Phys. Rev. Lett.* **100**, 026405 (2008).
 - ⁸ G. U. Oertzen and A. R. Gerson, *J. Phys. Chem. Solids* **68**, 324 (2007).
 - ⁹ P. J. D. Lindan, N. M. Harrison, M. J. Gillan, and J. A. White, *Phys. Rev. B* **55**, 15919 (1997).
 - ¹⁰ G. U. Oertzen and A. R. Gerson, *Int. J. Quantum Chem* **106**, 2054 (2006).
 - ¹¹ P. Krüger, S. Bourgeois, B. Domenichini, H. Magnan, D. Chandresis, P. L. Fèvre, A. M. Flank, J. Jupille, L. Floreano, A. Cossaro, A. Verдини, A. Morgante, *Phys. Rev. Lett.* **100**, 055501 (2008).
 - ¹² J. Ziegler, J. Biersack, and U. Littmark, *The stopping and range of ions in matter* (Pergamon, New York, 1985).
 - ¹³ F. Golmar, A. M. M. Navarro, C. E. R. Torres, F. H. Sánchez, F. D. Saccone, P. C. dos Santos Claro, G. A. Benítez, and P. L. Schilardi, *Appl. Phys. Lett.* **92**, 262503 (2008).
 - ¹⁴ A. Brinkman, M. Huijben, M. Van Zalk, J. Huijben, U. Zeitler, J. C. Maan, W. G. Van der Wiel, G. Rijnders, D. H. A. Blank, and H. Hilgenkamp, *Nat. Mater.* **6**, 493 (2007).
 - ¹⁵ G. Kopnov, Z. Vager, and R. Naaman, *Adv. Mater.* **19**, 925 (2007).
 - ¹⁶ C. Ronning, E. P. Carlsonb, and R. F. Davis, *Phys. Rep.* **351**, 349 (2001).
 - ¹⁷ S. P. S. Porto, P. A. Fleury, and T. C. Damen, *Phys. Rev.* **154**, 522 (1967).
 - ¹⁸ T. Ohsaka, F. Izumi, and Y. Fujiki, *J. Raman Spectrosc.* **7**, 321 (1978).
 - ¹⁹ A. Mooradian and P. M. Raccach, *Phys. Rev. B* **3**, 4253 (1971).
 - ²⁰ G. A. Samara and P. S. Peercy, *Phys. Rev. B* **7**, 1131 (1973).
 - ²¹ V. Swamy, B. C. Muddle, and Q. Dai, *Appl. Phys. Lett.* **89**, 163118 (2006).
 - ²² V. Maroni, *J. Phys. Chem. Sol.* **49**, 307 (1988).
 - ²³ G. R. Lumpkin, K. L. Smith, M. G. Blackford, B. S. Thomas, K. R. Whittle, N. A. Marks, and N. J. Zaluzec, *Phys. Rev. B* **77**, 214201 (2008).
 - ²⁴ M. Sterrer, E. Fischbach, T. Risse, and H.-J. Freund, *Phys. Rev. Lett.* **94**, 186101 (2005).
 - ²⁵ S. V. Chong, K. Kadowaki, J. Xia, and H. Idriss, *Appl. Phys. Lett.* **92**, 232502 (2008).
 - ²⁶ P. F. Chester, *J. Appl. Phys.* **32**, 2233 (1961).
 - ²⁷ E. Yamaka and R. G. Barnes, *Phys. Rev.* **135**, A144 (1964).
 - ²⁸ J. He, R. K. Behera, M. W. Finnis, X. Li, E. C. Dickey, S. R. Phillpot, and S. B. Sinnott, *Acta Mater.* **55**, 4325 (2007).
 - ²⁹ P. Dev, Y. Xue, and P. Zhang, *Phys. Rev. Lett.* **100**, 117204 (2008).